Large Scale Valorization Of Steel Slag Combined With Membrane-Based Direct Air Capture For Carbon Mineralization: A Techno-economic Evaluation†
Supporting Information

Vitor Gama[a‡], Kyle Shank[b‡], Madison Morgan[a], Owen Gerdes[a], Savannah Sakhai[a], Fernando V. Lima[a], Shang Zhai*[b,c], and Oishi Sanyal*[a]

[a] Chemical and Biomedical Engineering, West Virginia University, Morgantown, WV, USA
[b] Mechanical and Aerospace Engineering, The Ohio State University, Columbus, OH, USA.
[c] School of Earth Sciences, The Ohio State University, Columbus, OH, USA.
‡ These authors contributed equally to this work.

1 Supporting Figures

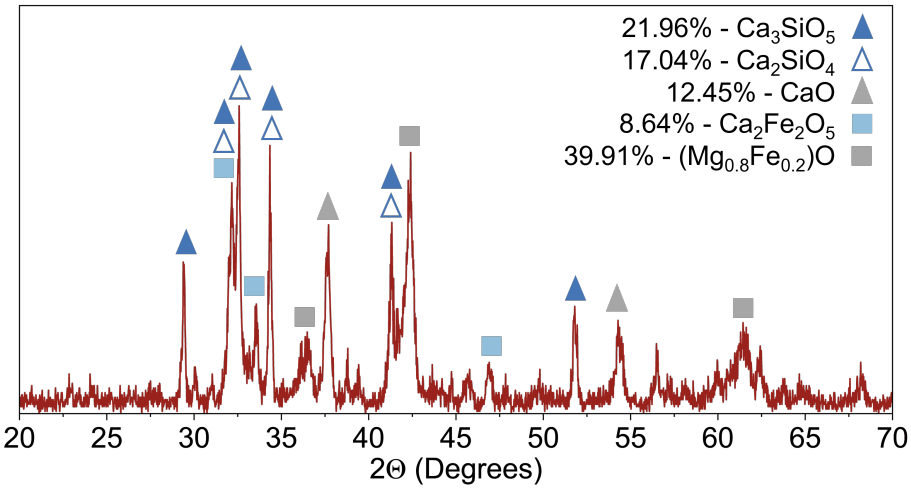

Figure S1 Steel Slag X-ray diffraction and Rietveld refinement.

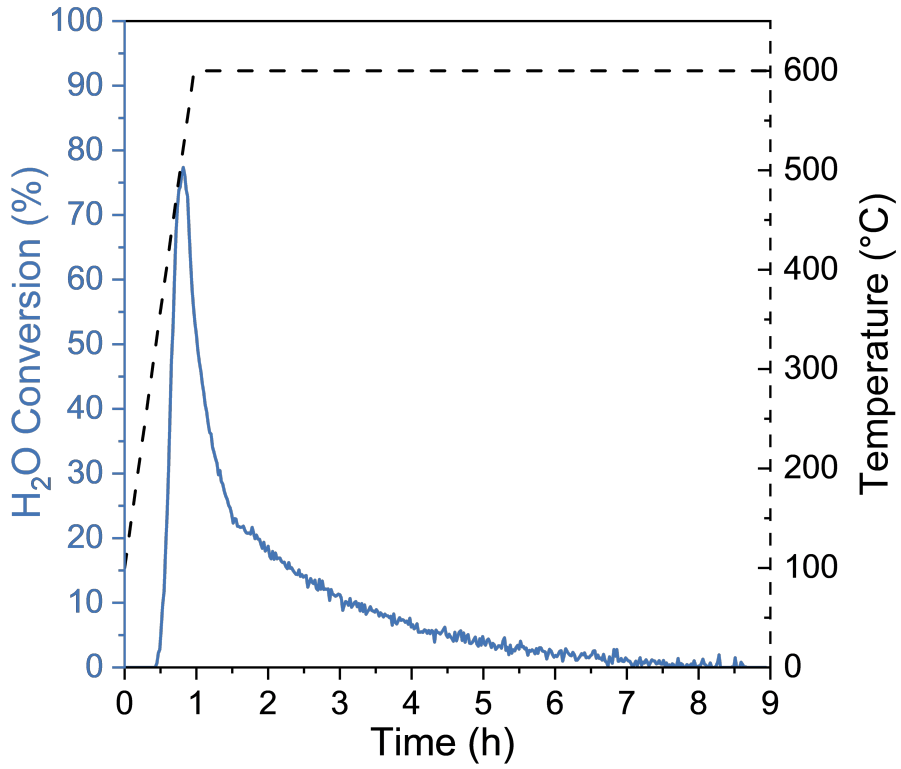

Figure S2 H_2 production performance with steel slag.

2 Mineralization Experimental Procedure

Samples of BOF steel slag were sourced from Cleveland-Cliffs – Cleveland Works. The slag was collected directly from the BOF prior to the slagging-off process. For preparation, large fragments were broken down with a sledgehammer to roughly 0.5 cm in size. 70 g of slag was then placed in a 75 ml alumina grinding jar equipped with a stainless steel sleeve, under an argon environment to limit exposure to air. Milling was performed in an Across International Desktop High Energy Vibratory Ball Mill for 30 minutes, followed

by a 20-minute rest, and then another 30-minute milling cycle. The resulting material was removed with a metal spatula and sieved through a 60-mesh (250 micron) screen. Any over sized material was first reduced using a 2 mm sieve; particles remaining too large were re-milled with the addition of fresh slag to bring the batch back to 70 g. The processed slag was stored under argon in a glove box until use.

Hydrogen production experiments were performed in a custom quartz tube (25 mm outer diameter and 609.6 mm length) containing a 3 mm thick G0 quartz frit (160–250 micron) positioned 15 mm off-center. 6 g of slag was packed between layers of quartz wool resting on the frit. The tube was placed vertically inside a Thermcraft Protégé XST split-tube furnace. A feed gas of 100 sccm composed of 2% H_2O vapor in argon (Cellkraft P-2 Humidifier) was passed through the slag. The furnace was ramped to 600 °C at 10 °C/min and held at that temperature for 8 hours to promote steam-to-hydrogen conversion. Gas products were analyzed with a gas chromatograph (Inficon Micro GC Fusion), with indicating Drierite installed upstream to capture excess water vapor and protect the GC. GC measurements began once the furnace reached 100 °C. After testing, the reacted slag was transferred back to the argon glovebox for storage.

For mineralization, experiments were conducted using 1% and 2% CO_2/Ar mixtures, with blank runs performed for comparison. Each experiment involved 3 cycles of two sequential steps: hydration followed by CO_2 mineralization. During hydration, 0.5 g of post-hydrogen production slag, 15 ml of deionized water (DI), and a stir bar were added to a 50 ml centrifuge tube. The tube was placed in a 250 ml beaker filled with 210 ml of water on a hot plate set to 108 °C, maintaining the water bath near 45°C. Stirring was performed at 400 rpm for 30 minutes. Afterward, the stir bar was removed from the centrifuge tube, and the mixture was centrifuged at 1200 rpm for 10 minutes.

During mineralization, the solution was transferred to a 20 ml glass vial with a stir bar, which was placed inside a 50 ml gas-washing bottle wrapped in 0.5-inch ceramic fiber insulation and maintained at 45 °C with a hotplate set to 63 °C and 300 rpm. The dip tube extended three-quarters into the solution, and the system was purged with argon before gas introduction. For CO_2 mineralization, a 40 sccm stream of either 1% or 2% CO_2/Ar was bubbled through the liquid for 15 minutes, followed by a 20-minute argon flush to dilute residual CO_2 within the bottle. The outlet gas was analyzed using a GC with Drierite upstream to remove water vapor. To synchronize measurements, GC sampling was initiated one minute before CO_2 introduction.

After each cycle, the solution was transferred to a fresh centrifuge tube, 0.5 g of post-hydrogen production slag was added, and the procedure was repeated. Any water lost to evaporation was added back to the solution after each cycle. At the end of each hydration and mineralization sequence, the temperature and pH were measured using a K-type thermocouple and an Ohaus Starter 2200 pH Bench Meter (ST322 electrode). Blank runs followed the same mineralization procedure, but with 15 ml of DI water in place of the slag-reacted solution.

3 Mineralization Mass and Energy Balances

To determine the molar amounts of reactive phases in steel slag during CO_2 mineralization, X-ray diffraction (XRD) of the steel slag was analyzed using Rietveld refinement. This method provided the relative proportions of crystalline phases in the slag (Figure S1). Among these, Ca_3SiO_5, Ca_2SiO_4, and CaO were identified as the primary phases contributing to CO_2 mineralization, while $Mg_{0.8}Fe_{0.2}O$ participated in H_2 generation and $Ca_2Fe_2O_5$ was considered inert. Because amorphous content cannot be directly measured with XRD, its influence was inferred from the experimental mineralization capacity. The mineralization capacity was obtained by multiplying the CO_2 conversion in the third reaction cycle by the total CO_2 supplied during that cycle. Figure 3 presents the CO_2 mineralization results for 1% and 2% CO_2 feeds, showing 55.4% and 43.3% conversion respectively. By comparing the measured CO_2 mineralization with the relative fractions of calcium-bearing phases (Eqs. 12-15), the reacted amounts of Ca_3SiO_5, Ca_2SiO_4, and CaO were determined. These values were then normalized to a 1 g basis to express the molar content of each phase per gram of slag.

The mass balance was initiated using the calculated quantities of Ca_3SiO_5, Ca_2SiO_4, and CaO. The required water volume for mineralization was scaled according to a 30:1 water-to-slag mass ratio. The FeO content in the slag was estimated from the experimentally measured H_2 production of 16.99 std. ml H_2 per gram of slag (Figure S2). The annual CO_2 mineralized was introduced into the system based on the DAC membrane output flow rate. Using these parameters, the mass balance was established and expressed on an hourly basis. The corresponding mass flows into and out of the system are summarized in Figure 4, alongside the process schematic.

The reactor heat balance was evaluated by accounting for heat losses through natural convection and the heat generated or consumed by exothermic and endothermic reactions. A cycle time of 15 minutes was assumed, consistent with the experimental CO_2 mineralization duration. Since the hydration step experimentally required 30 minutes, the system was modeled with two hydration reactors operating in parallel, each processing a quarter of the hourly mass flow and alternating a complete cycle every 15 minutes.

Reactor dimensions were determined from the material mass flow rates, with the reactors approximated as cubic vessels to estimate the external surface area. A slag density of 3000 $kg \cdot m^{-3}$ was assumed, while the density of hydrated slag was taken as 2604 $kg \cdot m^{-3}$ [1,2]. The effect of $Ca(OH)_2$ concentration on solution density was neglected, as a saturated solution has a density close to that of water[3]. The density of $CaCO_3$ was assumed to be 2700 $kg \cdot m^{-3}$ [4]. Heat loss to the surroundings was then estimated using the calculated reactor surface area and an overall heat transfer coefficient of 0.003 $kW \cdot (m^2 \cdot K)^{-1}$, representative of an insulated reactor in still air[5].

The thermal effect of the reactions was evaluated from the enthalpy of reaction and the number of moles of reactants processed in each cycle. The overall heat balance for the reactor was obtained by combining the convective heat loss through the reactor walls with the heat generated or consumed by the reactions.

Heat transfer between process steps was evaluated using literature values for enthalpy and specific heat capacities. The specific heat of steel slag was assumed to be 935 $J \cdot kg^{-1} \cdot K^{-1}$ [6]. Steel slag discharged from the BOF at 1650 °C was assumed to cool naturally to 653 °C, at which point the available sensible heat was sufficient to generate steam for the H_2 production step. Following steam reaction, the slag was cooled further to 45 °C to meet the temperature requirements of hydration. The sensible heat of slag transported on the conveyor was assumed to be fully lost to the atmosphere. Milling and filtration were modeled as isothermal steps at 45 °C.

Makeup water was assumed to enter the hydration reactor at 25 °C and required heating to 45 °C; however, this demand was less than the exothermic heat released during hydration. The density and specific heat of the outlet gas stream from the membrane separation unit were calculated using the ideal gas law. The overall heat balance is illustrated in Figure 4, with the individual heat transfer contributions summarized.

The H_2 production reactor was assumed to operate without external heat input or removal, as the heat loss to the environment approximately balanced the exothermic reaction heat. In contrast, the exothermic heat from the hydration reactor was managed via a heat exchanger. The outlet gas from the membrane unit entered at 25 °C and was assumed to absorb the reaction heat from the CO_2 mineralization step, increasing its temperature to approximately 36 °C. The analysis was performed under steady-state assumptions, and the initial heating of feed water was neglected.

The electrical energy demand of the process was estimated for the primary energy-consuming operations: the conveyor belt, milling, filtration, stirring, pumping, and flue gas handling. The conveyor belt power requirement was taken as 0.72 $kW \cdot Mg^{-1} \cdot h^{-1}$ per kilometer of horizontal transport[5]. The conveyor was designed to cool slag from the H_2 production outlet temperature to the hydration temperature. A belt width of 72 in (1.83 m) and a velocity of 3 $m \cdot s^{-1}$ were assumed from[7,8]. The slag was modeled as a flat plate with a constant cooling rate. Both radiative and convective heat transfer mechanisms were considered, with ambient conditions taken as air at 25 °C. Radiative heat transfer was calculated using a steel slag emissivity of 0.81[9]. Convective cooling was determined using the Nusselt number correlation for turbulent flow over a flat plate under constant heat flux conditions Eq. (S1)[10]. Heat transfer was evaluated using the average temperature approach Eq. (S2)[11]. The Reynolds number and convective heat transfer coefficient were calculated based on an initial conveyor length of 100 m, which was iteratively adjusted until convergence with the calculated length was achieved.

$$Nu_x = 0.0308\, Re_x^{4/5}\, Pr^{1/3} \tag{S1}$$

$$T_{\text{avg}} = \frac{T_{\text{in}}^5 - T_{\text{out}}^5}{5\,(T_{\text{in}} - T_{\text{out}})} \tag{S2}$$

Milling of steel slag was assumed to require 3.84 $kWh \cdot t^{-1}$, while filtration was estimated at 0.18 $kWh \cdot m^{-3}$ of water processed[12,13]. A filtration rate of 3 $L \cdot s^{-1} \cdot m^{-2}$ was assumed. Stirring energy for the hydration step was assumed to be 1.5 $kWh \cdot m^{-3}$ [5].

The pumping energy required to transfer the hydration reactor solution to the top of the spray tower was calculated based on the static and delivery head, neglecting frictional losses, and assuming an efficiency of 85%[14]. A pipe diameter of 0.2 m and a spray tower height of 7 m were used in the calculation[15]. The power demand for flue gas movement was estimated by assuming a pressure drop of 0.6 kPa across the spray tower and a fan efficiency of 88%[5,16]. The energy requirements for each unit operation are summarized in Figure 4.

4 Cost Estimation Breakdown

The techno-economic analysis uses a preliminary equipment cost estimation technique based on the capacity-exponent ("rule-of-thumb") scaling method described in Section 3.3.1 of the manuscript. In this approach, equipment purchase costs are estimated using reference costs based on characteristic design parameters such as power demands, heat-transfer surface area, flow rate, or reactor volume. While Table 2 in the main text enumerates the equipment and their respective sizing parameters used to calculate the estimates, the numerical values used in the scaling method are reported here to improve the cost estimation reproducibility. Tables S1-S2 summarize the equipment sizing parameters used for both process configurations evaluated in this study (1% and 2% CO_2 permeate streams). Values for the m-DAC subsystem collected directly from the AVEVA Process Simulation simulations, including compressor and vacuum pump duties, membrane area, heat-exchanger area, etc. The mineralization equipment sizes were determined from the scaled mass and energy balances of the hydrogen generation, slag hydration, and aqueous carbonation steps.

Table S1 Equipment list and capacity parameter values used for the cost estimation in the integrated m-DAC + mineralization system correspoding to the 1% CO_2 feed purity.

Equipment	Design parameter	Value	Units
m-DAC equipment			
Vacuum pump	Power	187	kW
Compressors (K1/K2/K3)	Power	137.9/131.52/131.4	kW
Heat exchangers (E1/E2/E3)	Heat-transfer area	174/174/100	m^2
Fan	Volumetric flow rate	30	$m^3\,s^{-1}$
Membrane module	Membrane area	1362.7	m^2
Mineralization equipment			
Water splitting reactor	Reactor volume	2.12	m^3
Mill	Solids throughput	8.59	$Mg\,h^{-1}$
Hydration reactor	Reactor volume	64.49	m^3
CO_2 capture spray tower	Gas flow rate	3088.19	$L\,s^{-1}$
Fan, centrifugal	Gas flow rate	3088.19	$L\,s^{-1}$
Pump, centrifugal	Liquid flow rate	70.75	$L\,s^{-1}$
Rotary drum filter — slag	Filter area	23.88	m^2
Rotary drum filter — $CaCO_3$	Filter area	23.58	m^2
Conveyor	Vendor reference index†	236901.51	dimensionless

Table S2 Equipment list and capacity parameter values used for the cost estimation in the integrated m-DAC + mineralization system correspoding to the 2% CO_2 feed purity.

Equipment	Design parameter	Value	Units
m-DAC equipment			
Vacuum pump	Power	100	kW
Compressors (K1/K2/K3)	Power	87.9/84.7/84.7	kW
Heat exchangers (E1/E2/E3)	Heat-transfer area	23/23/20	m^2
Fan	Volumetric flow rate	30	$m^3\,s^{-1}$
Membrane module	Membrane area	646.3	m^2
Mineralization equipment			
Water splitting reactor	Reactor volume	1.32	m^3
Mill	Solids throughput	5.36	$Mg\,h^{-1}$
Hydration reactor	Reactor volume	40.31	m^3
CO_2 capture spray tower	Gas flow rate	1834.20	$L\,s^{-1}$
Fan, centrifugal	Gas flow rate	1834.20	$L\,s^{-1}$
Pump, centrifugal	Liquid flow rate	44.22	$L\,s^{-1}$
Rotary drum filter — slag	Filter area	14.93	m^2
Rotary drum filter — $CaCO_3$	Filter area	14.74	m^2
Conveyor	Vendor reference index†	44135.03	dimensionless

5 Limited Recovery Simulations

In order to outline the limitations of the base case system, this section highlights the prohibitive outcomes from this baseline simulation. The process simulation parameters were similar to ones described in section 3.1.1. However, the intrinsic properties values were set based on the regressed D_{CO_2} and K_{eq}. These base values, although derived from an existing membrane, when introduced in the simulation do not lead to an desired outcome in terms of CO_2 recovery. Figure S3 shows the flowsheet simulated in APS considering $D_{CO_2} = 3.8\times10^{-11}$ and $K_{eq} = 2.6\times10^{-5}$.

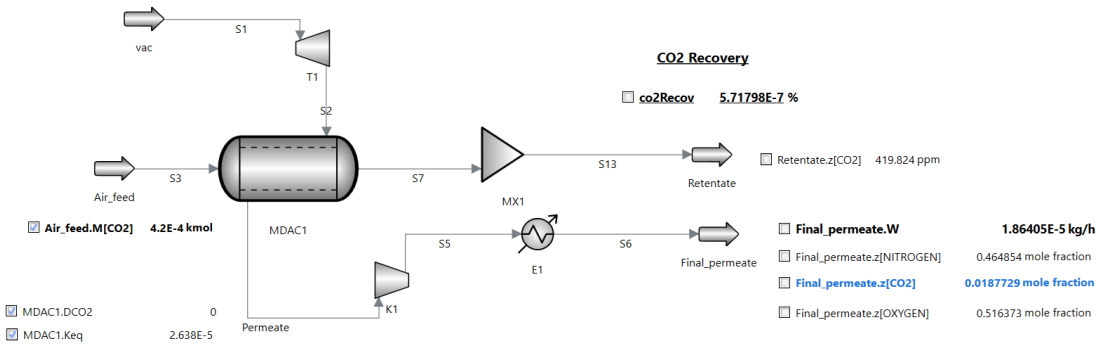

Figure S3 Simulation flowsheet of the m-DAC system using base case membrane properties

Even though the CO_2 concentration reached nearly 2% (highlighted in blue in Figure S3), the corresponding recovery remains on the order of 10^{-7}%, which is for all practical purposes negligible. This makes the configuration fundamentally unsuitable for techno-economic evaluation, particularly given the imposed constraint of achieving at least 1000 tons of CO_2 captured per year. Therefore, the baseline scenario should not be interpreted as commercially viable under current conditions. Instead, it represents an aspirational upper-bound case that highlights the gap between current system performance and the requirements for meaningful large-scale CO_2 capture. At present, a viable system would require significant advances in membrane performance, process design, and cost reduction alternatives. Accordingly, this scenario is best interpreted as a reference point for identifying performance improvement pathways, rather than as an indication of near-term feasibility.

Notes and references

[1] M. Díaz-Piloneta, M. Terrados-Cristos, J. V. Álvarez Cabal and E. Vergara-González, *Materials*, 2021, **14**, 3587.

[2] A. J. Allen, J. J. Thomas and H. M. Jennings, *Nature Mater*, 2007, **6**, 311–316.

[3] R. G. Bates, V. E. Bower and E. R. Smith, *J. RES. NATL. BUR. STAN.*, 1956, **56**, 305.

[4] S. Teir, S. Eloneva and R. Zevenhoven, *Energy Conversion and Management*, 2005, **46**, 2954–2979.

[5] D. R. Woods, *Rules of Thumb in Engineering Practice*, Wiley, 1st edn., 2007.

[6] J. Wang and Y. Huang, *Journal of Cleaner Production*, 2023, **395**, 136289.

[7] *High Speed Conveyors | Conveying Solutions | Dorner*, 2025, `https://www.dornerconveyors.com/solutions/high-speed-conveyors`.

[8] *Industrial Belt Conveyors & Powered Conveyor Belt Systems*, 2025, `https://heinrichbrothers.com/product/conveyor-systems/belt-conveyors/`.

[9] B. V. Rangavittal, H. Köchner and B. Glaser, *steel research int.*, 2025, **96**, 2400277.

[10] T. L. Bergman and A. S. Lavine, *Fundamentals of heat and mass transfer*, John Wiley & Sons, Eighth edition edn., 2017.

[11] V. K. Budama, N. G. Johnson, I. Ermanoski and E. B. Stechel, *International Journal of Hydrogen Energy*, 2021, **46**, 1656–1670.

[12] M. Grzegorzek, K. Wartalska and B. Kaźmierczak, *International Communications in Heat and Mass Transfer*, 2023, **143**, 106674.

[13] E. Mundy, *RMG Letter Draft*, 2024.

[14] V. K. Arun Shankar, S. Umashankar, S. Paramasivam and N. Hanigovszki, *Applied Energy*, 2016, **181**, 495–513.

[15] D. W. Keith, G. Holmes, D. St. Angelo and K. Heidel, *Joule*, 2018, **2**, 1573–1594.

[16] X. Liu, Q. Dang and G. Xi, *Engineering Applications of Computational Fluid Mechanics*, 2008, **2**, 130–140.